Spatial Patterns in Catchment Hydrology

Observations and Modelling

Edited by

RODGER GRAYSON

University of Melbourne

GÜNTER BLÖSCHL

Technische Universität Wien

CAMBRIDGE
UNIVERSITY PRESS

PUBLISHED BY THE PRESS SYNDICATE OF THE UNIVERSITY OF CAMBRIDGE
The Pitt Building, Trumpington Street, Cambridge, United Kingdom

CAMBRIDGE UNIVERSITY PRESS
The Edinburgh Building, Cambridge, United Kingdom
40 West 20th Street, New York, NY 10011–4211, USA
10 Stamford Road, Oakleigh, Melbourne 3166, Australia
Ruiz de Alarcón 13, 28014 Madrid, Spain
Rock House, The Waterfront, Cape Town 8001, South Africa

http://www.cup.org

First published 2001

Printed in the United Kingdom at the University Press, Cambridge.

Typefaces Times New Roman PS 10.5/13 and Helvetica Neue Condensed *System* 3B2 [KW]

A catalogue record for this book is available from the British Library

Library of Congress Cataloguing-in-Publication Data

Spatial patterns in catchment hydrology : observations and modelling / edited by Rodger Grayson, Günter Blöschl.
p. cm.
ISBN 0-521-63316-8
1. Watersheds–Mathematical models. 2. Hydrology–Mathematical models. 3. Spatial analysis (Statistics) I. Grayson, Rodger, 1963–II. Blöschl, Günter, 1961–

GB980.S66 2001
551.48′01′5118–dc21 00-040357

Contents

Spatial Patterns in Catchment Hydrology

Observations and Modelling

For many years now, modelling tools have been available to simulate spatially distributed hydrological processes. These tools have been used for testing hypotheses about the behaviour of natural systems, for practical applications such as erosion and transport modelling, and for simulation of the effect of land use and climate change. However, so far the quality of the simulations and spatial process representations has been difficult to assess because of a lack of appropriate field data.

Spatial Patterns in Catchment Hydrology: Observations and Modelling brings together a number of recent field exercises in research catchments, that illustrate how the understanding and modelling capability of spatial processes can be improved by the use of observed patterns of hydrological response. In addition the introductory chapters review the nature of the hydrological variability, and introduce basic concepts related to measuring and modelling spatial hydrologic processes. This introductory material provides the conceptual and theoretical background needed to move into this exciting area of research for a general earth sciences/water engineering audience. The book demonstrates that there is rich information in patterns that provide much more stringent tests of the models and much greater insight into hydrological behaviour than traditional methods.

Written in an intuitive and coherent manner, the book is ideal for researchers, graduate students and advanced undergraduates in hydrology, and a range of water related disciplines such as physical geography, earth sciences, and environmental and civil engineering as related to water resources and hydrology.

Rodger Grayson is an Associate Professor and Senior Research Fellow at the Center for Environmental Applied Hydrology and the Cooperative Research Center for Catchment Hydrology, both of which are in the Department of Civil and Environmental Engineering at the University of Melbourne. His professional interests include research, teaching and consulting related to environmental hydrology, the modelling and monitoring of water quality and quantity from research catchment to continental scales, and integrated catchment management. He has published over 100 papers and reports in international and national journals and conferences, as well as an edited book, several book chapters and this current book. He is an associate editor of *Water Resources Research* and the *Journal of Hydrology*.

Günter Blöschl is an Associate Professor at the Institute of Hydraulics, Hydrology and Water Resources Management of the Technical University of Vienna. His professional interests include measuring and modelling spatial hydrologic processes at a range of scales as well as engineering hydrology and water resources management. He is an author of over 100 scientific papers and has received the Schrödinger and Lise Meitner awards from the Austrian Science Foundation. He is an associate editor of *Water Resources Research*, the *Journal of Hydrology* and an editorial board member of *Environmental Modelling and Software*. He is a Vice President of sections of both the European Geophysical Society and the International Association of Hydrological Sciences.

6

Runoff, Precipitation, and Soil Moisture at Walnut Gulch

Paul Houser, David Goodrich and Kamran Syed

6.1 INTRODUCTION

The research presented here was undertaken at the Walnut Gulch Experimental Watershed (30°43′N, 110°41′W) near Tombstone, Arizona, which is operated by the Southwest Watershed Research Center (SWRC), Agriculture Research Service (ARS), U.S. Department of Agriculture (USDA). The extremes in rainfall and temperature in this region lead to great spatial heterogeneity in soil hydrological processes. Observations from a series of nested gauging stations, a dense network of precipitation gauges, and remotely sensed soil moisture estimates, in concert with specialised remote sensing, surface characterisation, and numerical simulation have led to numerous insights into the nature, causes, and effects of hydrologic spatial patterns in this semi-arid catchment. The nature, representation, and interrelation of spatial rainfall patterns and their impact on the spatial distribution of runoff and soil moisture is described. Additionally, the representation of this spatial behaviour through the integration of observations in a distributed hydrologic model using data assimilation methods is assessed.

6.1.1 Description of Study Area

The Walnut Gulch Experimental Watershed (Figures 6.1 and 6.3) was selected as a research facility by the United States Department of Agriculture (USDA) in the mid-1950s. Prior appropriation water laws resulted in conflicts between upstream land owner conservation programs and downstream water users. Technology to quantify the influence of upland conservation on downstream water supply was not available. Thus, scientists and engineers in USDA selected Walnut Gulch for a demonstration/research area that could be used to monitor and develop technology to address the problem. In 1959, facilities needed for soil and water research in the USDA were identified in a United

Rodger Grayson and Günter Blöschl, eds. *Spatial Patterns in Catchment Hydrology: Observations and Modelling*

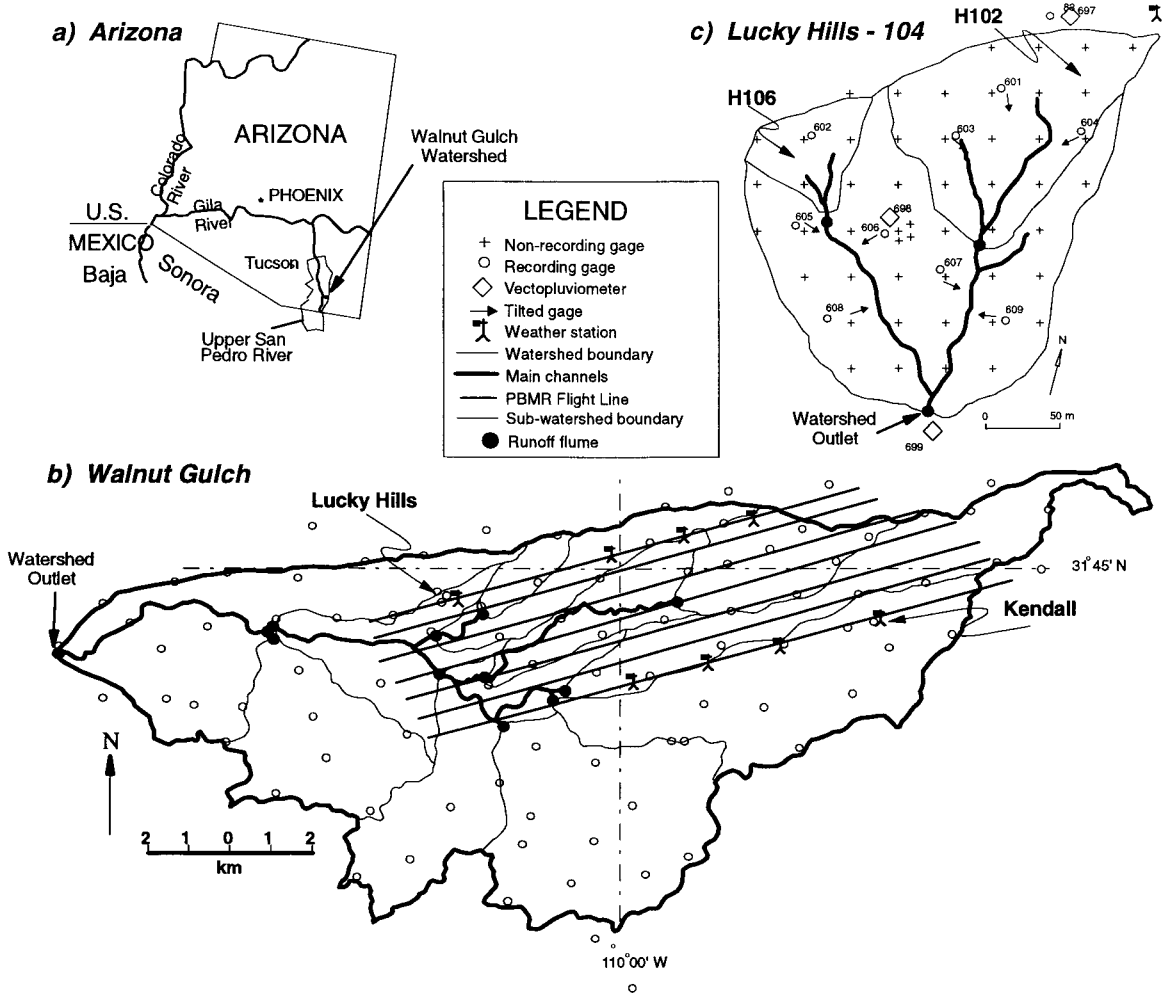

Figure 6.1. The Walnut Gulch Experimental Watershed: (a) location map; (b) catchment map including raingauges, major drainages, runoff flumes, flight lines; and (c) Lucky Hills subcatchment map.

States Senate Document (U.S. Senate Committee, 1959). The Southwest Watershed Research Center in Tucson, Arizona, USA, was created in 1961 to administer and conduct research on the Walnut Gulch watershed (Renard et al., 1993).

The Walnut Gulch Experimental Watershed (WGEW) is defined as the upper 148 km^2 of the Walnut Gulch drainage basin in an alluvial fan portion of the San Pedro catchment in southeastern Arizona (Figure 6.1). Depth to ground water varies from 45 m at the lower end to 145 m in the centre of the catchment. Soil types range from clays and silts to well-cemented boulder conglomerates, with the surface (0–5 cm) soil textures being gravelly and sandy loams containing, on average, 30 % rock and little organic matter (Renard et al., 1993). The topography can be described as gently rolling hills incised by steep drainage channels which are more pronounced at the eastern end of the catchment near the Dragoon Mountains. The mixed grass-brush rangeland vegetation, which is typical of southeastern Arizona and southwestern New Mexico, ranges from 20 to 60 % in coverage. Grasses primarily cover the eastern half of the catchment, while the western half is bush-dominated.

This rangeland region receives 250–500 mm of precipitation annually, with about two-thirds of it as convective precipitation during a summer monsoon season. The balance of precipitation falls during winter frontal storms of Pacific origin (Figure 6.2) and potential evapotranspiration is approximately ten times annual rainfall. The runoff in the ephemeral streams is of short duration and is typically near critical depth (Renard et al., 1993).

Currently, eighty-five recording rain gauges, eleven primary catchment runoff-measuring flumes, and two micrometeorological observation (Metflux) stations make the WGEW a valuable research location. During Monsoon '90 (July 23 to August 10, 1990), eight Metflux stations provided continuous measurement of local meteorological conditions and the surface energy balance, and extensive remote-sensing observations were made (Kustas and Goodrich, 1994). Figure 6.3 shows some of the monitoring equipment and gives an impression of the landscape.

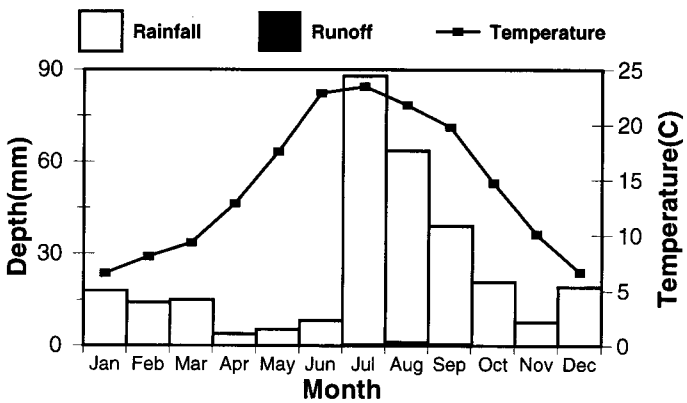

Figure 6.2. Monthly average temperature, rainfall, and runoff for the Walnut Gulch Experimental Watershed.

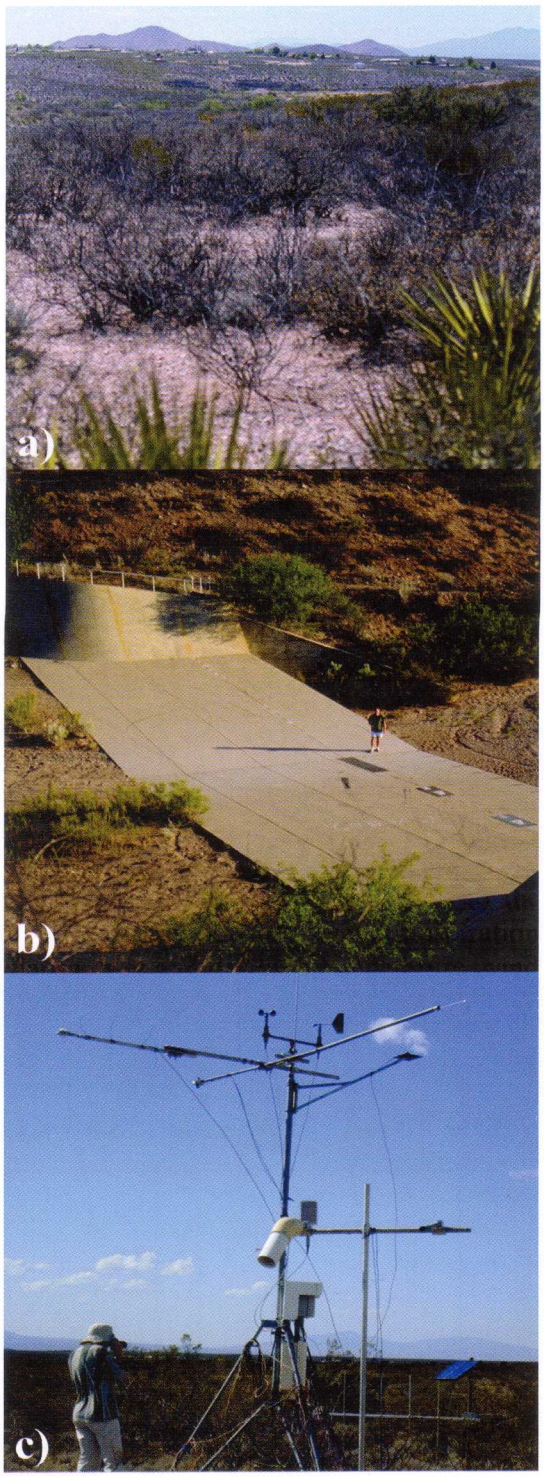

Figure 6.3. Mosaic of three photos of the WGEW: (a) catchment landscape, with the city of Tombstone, Arizona in the distance; (b) a large runoff measurement flume; and (c) the Lucky Hills metflux site.

6.1.2 Review

Many recent studies of hydrologic variability have shown that land surface heterogeneity has a profound impact on hydrologic phenomena (Milly and Eagleson, 1988; Pitman et al., 1990; Avissar, 1992). Spatial and temporal variability in meteorology (precipitation, wind speed, humidity, radiation, and temperature), soils (hydraulic conductivity, porosity, water retention, topography, and thermal properties), and vegetation (stomatal resistance, leaf area index, albedo, and root depth) interact in a highly nonlinear manner to produce complex heterogeneity in soil moisture, runoff, and evapotranspiration (Ghan et al., 1997). Detailed analysis of surface observations have provided valuable insights into the nature and causes of surface heterogeneity (Seyfried and Wilcox, 1995). It is well established that variability in precipitation is among the most important causes of variability in soil moisture and runoff (Ghan et al., 1997). However, because soil moisture integrates the temporal variability of precipitation, knowledge of the instantaneous precipitation distribution does not necessarily provide a complete picture of hydrologic variability. The interrelations between the complex processes causing hydrologic variability also change in time and space (Seyfried and Wilcox, 1995).

Physically-based hydrologic models have great potential for helping to unravel the complexities of hydrologic heterogeneity, by helping us to critically analyse the problem, organise our thoughts and data sets, and to test our hypotheses. Modelling the impact of meteorologic, soils, and vegetation heterogeneity on surface hydrology has taken two general directions: (1) *spatially distributed modelling* that uses spatially distributed inputs of relevant soil, vegetation, and meteorology to enable better prediction of hydrologic patterns; and (2) *statistical-dynamical modelling* approaches in which homogenous land patches are identified and modelled as a single unit. This facilitates the development of probability density functions, that when combined with the physically-based hydrologic equations, characterise the variability of the hydrologic system (Avissar, 1992).

Numerous studies have investigated the nature and prediction of hydrologic spatial variability at Walnut Gulch (Kustas and Goodrich, 1994; Schmugge et al., 1994; Goodrich et al., 1994, 1995; Humes et al., 1997; Syed, 1994; Jackson et al., 1993; Michaud and Sorooshian, 1994b; Houser et al., 1998, 2000. Generally, these studies have shown that the highly convective, and therefore spatially variable nature of precipitation, has profound impacts on the spatial distribution of soil moisture and temperature, the production of runoff, and the partitioning of the surface energy balance. The variability of soils and vegetation were generally found to have a second-order modifying effect on the spatial variability imposed by precipitation, and at high resolutions, surface temperatures and fluxes were found to be strongly correlated with topography.

This chapter summarises the work on characterisation and simulation of spatial variability of soil moisture and runoff in response to spatial precipitation patterns at the WGEW. First, a discussion of patterns and characteristics of

precipitation, soil moisture and runoff based on observations is presented in Section 6.2. This is followed in Section 6.3 with a discussion of modelling and spatial inferences of precipitation, soil moisture, and runoff.

6.2 OBSERVATIONS

6.2.1 Observed Spatial and Temporal Characteristics of Walnut Gulch Precipitation

Knowledge of spatial and temporal characteristics of rainfall is crucial for better understanding this important component of the hydrologic cycle and to represent it more realistically in rainfall-runoff models. Various spatial storm characteristics which are considered important in runoff production of a catchment include, but are not limited to, areal storm coverage, its intensity patterns, direction of storm movement (Osborn, 1964), its position within the catchment (Michaud, 1992), and the extent and intensity of the runoff-producing storm core (Koterba, 1986).

There are three factors which generally limit the reliability of these computed spatial rainfall measures. First, there are inherent limitations in the data-collection procedures. The raingauge design, technician experience, and digitising methodology play important roles in establishing the accuracy of the data. Second, WGEW rainfall is observed at points scattered over a finite area. The interpolation techniques generally used to generate a continuous representation from point data have limitations. Third, interpretation of computed measures may differ depending on the interpolation method used. It is appropriate to devote some discussion to these limitations before describing the observed spatial nature of rainfall in detail because precipitation is such a dominant driver of catchment hydrology at the WGEW (see also Chapter 2 for a general discussion of interpolation issues).

In Walnut Gulch, rainfall observations from more than ninety gauges are available (Figure 6.1b). These are standard weighing type gauges that record the cumulative depth of precipitation continuously as a line trace on a revolving chart driven by an analog clock. The chart completes one revolution in 24 hours and remains in place for seven days before it is replaced with a fresh chart. These charts are manually checked and inferred for starting and ending times of rainfall events. To identify spatial rainfall patterns, the point observations must be transformed to a relatively continuous field, which is achieved by using spatial interpolation methods. Several methods of interpolation are available and each has its strengths and weaknesses which are thoroughly documented in the literature (Myers, 1994) and discussed in Chapter 2, pp. 26–45.

An analysis of Walnut Gulch rainfall data and a mathematically defined synthetic surface showed that both kriging and multiquadric interpolation methods (Shaw and Lynn, 1972) such as splines, produce similar results based on cross-validation residuals. Given these results, the multiquadric method was

used here because it does not require a labor-intensive a priori definition of a variogram or correlogram.

A total of 302 summer thunderstorm events that occurred in the period from 1975 to 1991 were analysed, 85 of which produced runoff at the outlet of the catchment. An event was defined as a rainfall episode separated from other rainfall episodes by at least 1 hour. The rainfall data from all 91 gauges was discretised into 10 minute time slices and then used in the multiquadric interpolation process to estimate rainfall values on a 100 m grid covering the entire catchment which were used to compute the storm areal coverage, position, and movement at a range of subcatchment scales.

At the Lucky Hills catchment scale (< 5 hectares), the assumption of spatially uniform rainfall was tested by making measurements with 10 recording and 49 non-recording raingauges, 9 tilted non-recording gauges, and 3 vectopluviometers for a range of events during the 1990 monsoon season (Figure 6.1c). The data were analysed to: 1) assess the precipitation measurement uncertainty due to gauge type, calibration, data reduction and placement; 2) assess the impacts of wind on precipitation observations; and 3) evaluate the impact of spatial and temporal rainfall variability on the estimate of areal precipitation over the catchment.

A histogram of areal total storm coverage for the 302 events is plotted in Figure 6.4a. Slightly less than half the total number of storms cover the entire 148 km^2 catchment. An event rarely delivers rain to the entire catchment instantaneously, but may affect large portions of the catchment over its entire duration. The contrast between total storm areal coverage and within storm coverage is illustrated in Figure 6.4b. The local nature and high spatial variability of these convective storms is evident. About one-third of storms occur in the range of 30 to 50 km^2 and about half are greater than 50 km^2 with a maximum of 120 km^2. The spatial extent of storm cores was found to be even more limited. Out of a total of 302 events, 53 events contained a high-intensity storm core (10 minute intensity > 25 mm/hr), of which about 25 % were in the range of areal coverage of 2 to 3 km^2, 50 % ranged from 3 to 9 km^2 and the remaining 25 % were larger than 9 km^2 with a maximum of 34 km^2.

It is also interesting to observe how these storms, on average, grow and decay in time. To examine this, the average of areal coverage of all storms for each 10 minute time step was computed from a common start time (Figure 6.5). The dotted line is the result of averaging every storm whether or not it reported any rain in a particular 10 minute interval (n was always 302). The rapid growth of the areal coverage of a storm and its recession are shown in Figure 6.5. When only those events that reported some rain in a particular time step were averaged, the first 1.5 hours was largely unchanged, indicating that most of the storms last more than 1.5 hours. However, beyond 1.5 hours, there is a sharp deviation, indicating that the longer duration storms have substantial spatial coverage (greater than 50 km^2). When the average rainfall volume in successive time steps was plotted in a similar fashion, its shape was very similar to the areal coverage plot except that

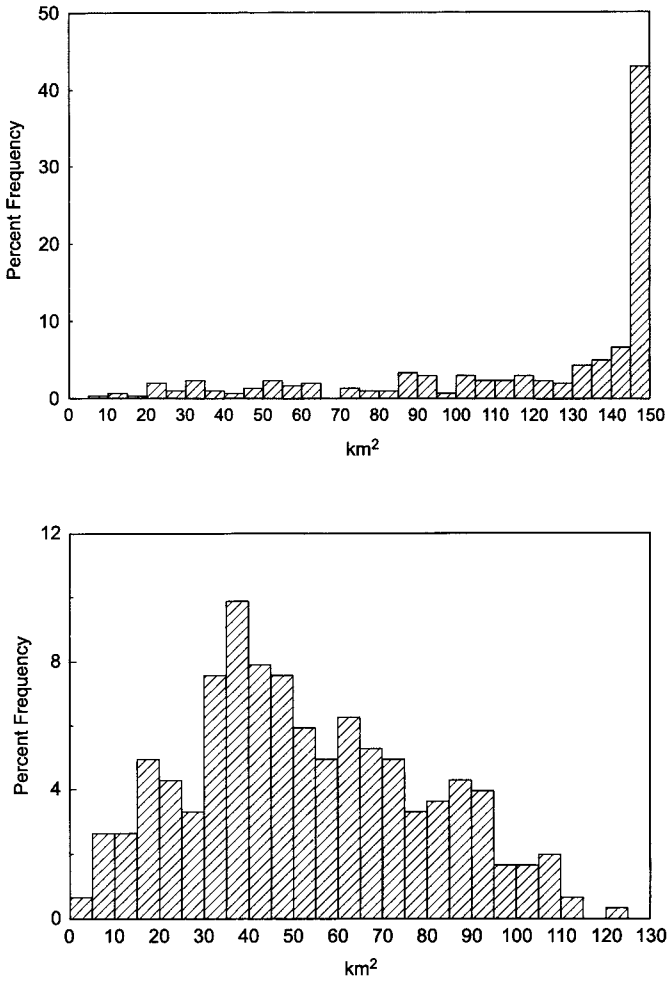

Figure 6.4. (a) Spatial storm coverage on an event basis. (b) Spatial storm coverage averaged for 10 minute time increments through storm duration.

its peak occurred at 70 minutes. This indicates that rainfall intensities typically peak in the first 1.5 hours of the storm even though the average storm event lasts for 4.75 hours.

Due to the limited extent of runoff producing storm intensities and high runoff transmission losses, the location of the storm core within the catchment is also very important. An example is shown in Figure 6.6 for a storm that occurred on July 30, 1989. The storm had two distinct periods of high-intensity rainfall (Figure 6.6a). The first one occurred near the start of the event, and was located near the catchment outlet (Figure 6.6b). This was followed by a low-intensity period of about 90 minutes. The second high-intensity burst then occurred, and was located near the head of the catchment (Figure 6.6c). This example clearly illustrates that, in this environment, it may be difficult to uniquely define a rainfall event using the arbitrary criteria currently utilised in

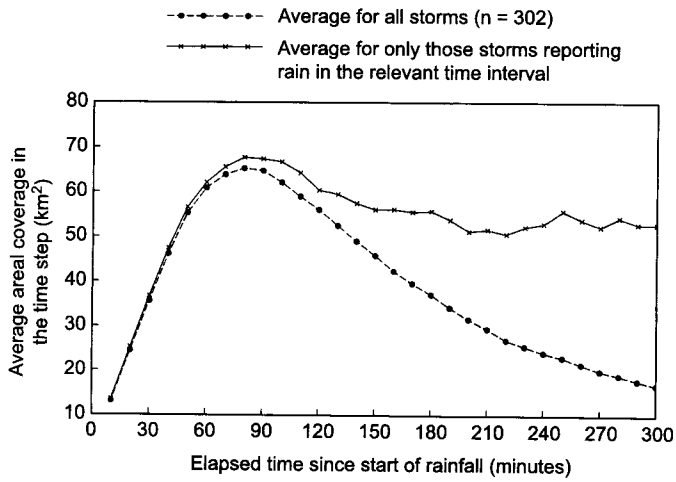

Figure 6.5. Progression of average spatial storm extent within event duration.

Walnut Gulch data processing, as these two periods of high-intensity rainfall are likely to have been two independent thunderstorm cells.

At the small-catchment scale, the intensive observations made at Lucky Hills – 104 resulted in several significant findings. It was found that the range of observed variation over the catchment was greater than the variation that would result from total measurement error (i.e. even at this scale spatial variability exists). An example of a storm (August 12, 1990) exhibiting the largest absolute variation in rainfall over the 4.4 hectare Lucky Hills – 104 catchment is shown in Figure 6.7. In addition, geostatistical analysis indicated the presence of first-order drift with corresponding rainfall gradient ranges from 0.28 to 2.48 mm/100 m with an average of 1.2 mm/100 m. These gradients represent a 4 % to 14 % variation of the mean rainfall depth over a 100 m distance indicating that raingauge location is particularly important if only one gauge is available. This suggests that the typical uniform rainfall assumption is *invalid* at the 5 hectare scale in regions where convective thunderstorm rainfall is significant. Spatial rainfall variation at this scale is attributed to localised wind effects from down drafts associated with the relatively random location of air mass thunderstorms in relation to the catchment. The overall WGEW raingauge network depicted in Figure 6.1b will not be able to resolve the rainfall spatial variations and patterns at the 5 hectare catchment scale for storms such as those illustrated in Figure 6.7. However, the density of the large area network is such that overall gradients in rainfall depth of typical air mass thunderstorms are captured. This should allow approximate estimation of the first-order drift noted for all but one of the storms observed with the small area network at Lucky Hills. While it may be possible to estimate gradients in rainfall depth with the large area network, rainfall maxima or minima occurring between the gauges will not be resolved at the 5 hectare scale. Spatial rainfall variation at this scale has important implications as testing and validation of process-based hydrologic models are often conducted on small research catchments using the spatially uniform rainfall assumption (single rain-

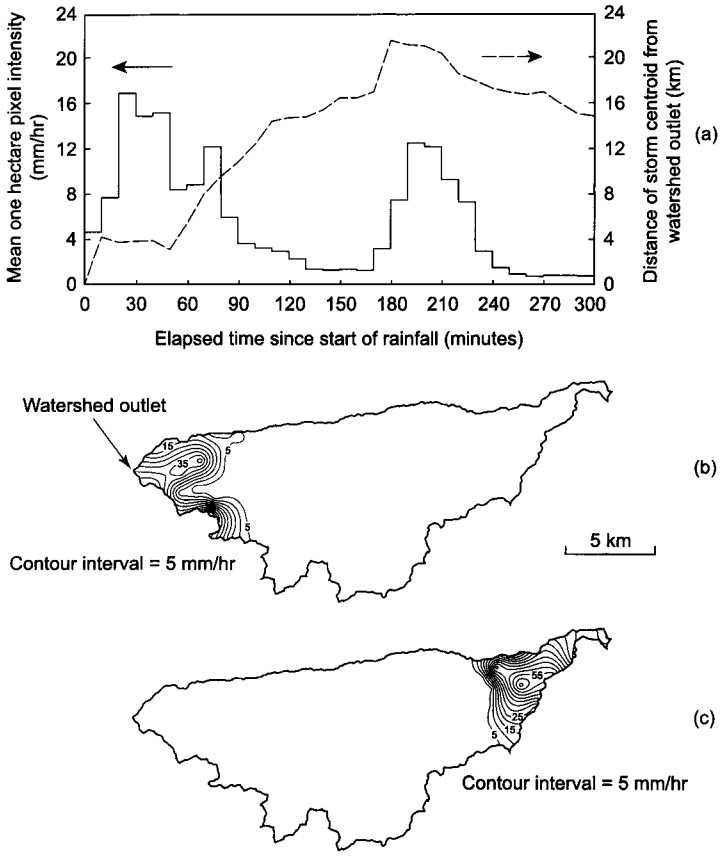

Figure 6.6. An example of spatial and temporal separation of high-intensity storm cells. (a) Spatially averaged storm intensities (solid line) and storm centroidal position (dashed line) in 10 minute time increments for the event of July 30, 1989. (b) Intensity contours during 40–50 minute interval. (c) Intensity contours during 190–200 minute interval.

gauge). The impacts of observed rainfall variability on runoff modelling at this scale are discussed in Section 6.3.3.1.

6.2.2 Observed Spatial and Temporal Characteristics of Walnut Gulch Soil Moisture

In Walnut Gulch, soil moisture observations were made by in-situ gravimetric sampling, resistance sensors, and Time Domain Reflectometry (TDR) sensors, as well as by microwave remote sensing. During Monsoon '90, three replicate gravimetric surface soil moisture samples were collected daily at the eight Metflux sites (Schmugge et al., 1994). These were converted to volumetric soil moisture using bulk density measurements made at each site. The only continuous soil moisture measurements made during Monsoon '90 were those made with resistance sensors (Kustas and Goodrich, 1994). They were placed at 2.5 cm and 5 cm below the surface at all eight Metflux sites. These sensors are generally difficult to

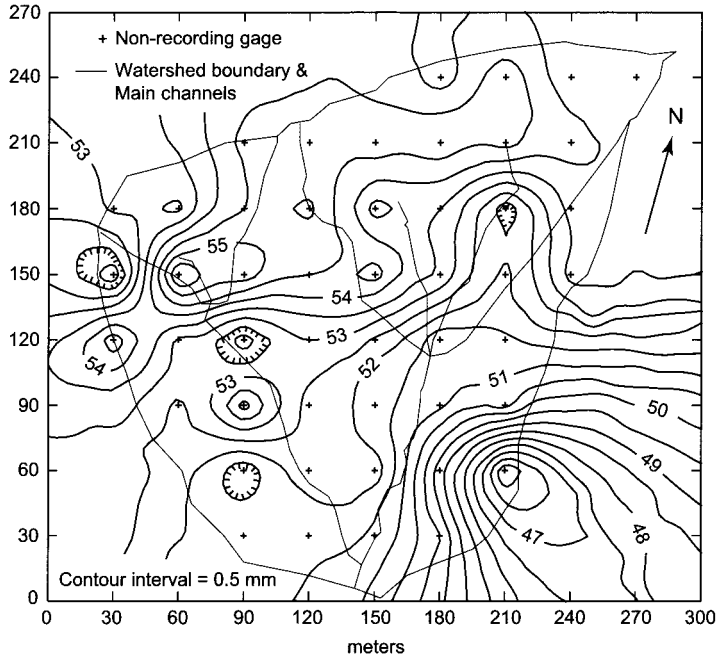

Figure 6.7. Contour map of the rainfall depth for the storm of August 12, 1990 (interpolation by isotropic kriging). Storm duration is 4 hours 42 minutes with about 75 % of the rain falling in 26 minutes.

calibrate and tend to drift. Therefore, following the recommendation of Stannard et al. (1994), the resistance data were calibrated against the gravimetric samples and then used to interpolate gravimetric data to each model time step. TDR measurements were made at daily intervals and at multiple depths down to 0.5 m at two of the Metflux sites (Kustas and Goodrich, 1994).

Engman (1991) described NASA's 21 cm wavelength (1.42 GHz), passive microwave Push Broom Microwave Radiometer (PBMR) instrument as "a mature and reliable instrument with a good history of soil moisture measurements". This approach relies on the large dielectric contrast between water and dry soil at long (> 10 cm) microwave wavelengths that causes the soil's emissivity to be a function primarily of moisture content. Vegetation can reduce the range of microwave brightness variation, totally obscuring the soil moisture signal if it is present in sufficiently large amounts. Fortunately this remote-sensing technique works well because Walnut Gulch has minimal vegetation (Schmugge et al., 1994).

During the Monsoon '90 field campaign (July 23 to August 10, 1990), the PBMR instrument was flown on board the National Aeronautics and Space Administration (NASA) C-130 aircraft. Six days (July, 31 August 2, 4, 5, 8 and 9, 1990) of microwave brightness temperature were collected over an 8 × 20 km area in the northeastern portion of the catchment (Schmugge et al., 1994). The period was very dry prior to the first flight, which was followed by 5 cm of rain falling over most of the study area on August 1, 1990. This

produced a significant decrease in brightness temperature (50 to 60 K) on August 2, 1990. The successive flights on August 4, 5, 8, and 9, 1990 showed the effects of some smaller rain storms and drydown of the area. A strong east-west spatial pattern is also evident and is strongly correlated to the observed soil and vegetation gradients. The changes in brightness temperature at six of the eight Metflux sites (Figure 6.1b) were well correlated with rainfall ($R^2 > 0.9$) and in-situ soil moisture ($R^2 = 0.8$) (Schmugge et al., 1994). The linear relationships established between microwave brightness temperature and gravimetric soil moisture at each Metflux site by Schmugge et al. (1994) were used with an inverse distance weighting scheme to invert microwave brightness temperature to soil moisture (Figure 6.8) (Houser et al., 1998).

The PBMR data have been analysed using geostatistical methods (see Chapter 2). The analysis also showed that the correlation structure varies with time. The July 31, 1990 PBMR observations, taken during dry conditions, show little spatial correlation, i.e. there is only very short range correlation probably due to random pattern of surface properties. One day after the large precipitation event on August 1, 1990, the variogram changes to linear with a very small nugget and a range beyond the observation area (15 km), i.e. the storm pattern imposes a large-scale pattern on the brightness temperature. Three days after the August 1, 1990 storm, a range of about 3.5 km becomes apparent, that is, as the surface dries, the scale of correlation decreases. Eight days after the storm, some spatial structure is still evident in the PBMR variogram but there are also significant random components in the pattern (Houser et al., 1998), i.e. the brightness temperature pattern imposed by the storm is disappearing and the random pattern of surface properties is dominating again.

A multispectral scanner was also flown on NASA's C-130 aircraft during the Monsoon '90 field experiment. Using the NS001 thermal band (10.9–12.3 μm), in conjunction with a radiative transfer algorithm (LOWTRAN 7) that corrected for atmospheric effects on the signal, surface temperature distributions were derived (Figure 6.8) (Humes et al., 1997). The image on August 1, 1990 shows areas of low temperatures corresponding to isolated cumulus clouds. There are also clear discontinuities between the two flight lines, which are attributed to the time difference in data acquisition (see Humes et al., 1997). It is clear that the surface temperature is strongly influenced by the surface soil moisture since it has a high correlation with both the PBMR observations and the rainfall distribution, and also shows the effects of shading by topography and larger amounts of vegetation in drainage lines.

In addition to the Monsoon '90 PBMR remotely sensed and ground-based gravimetric measurements, a similar suite of measurements was carried out over Walnut Gulch in 1991 using ESTAR, the airborne electronically steered thinned array L-band radiometer (Jackson et al., 1993). As in 1990, a wide range of soil moisture patterns and conditions were captured as flights were made before and after several significant rainfall events. With the ground-based data as well as the patterns of soil moisture acquired in 1990 by the PBMR instrument, the viability

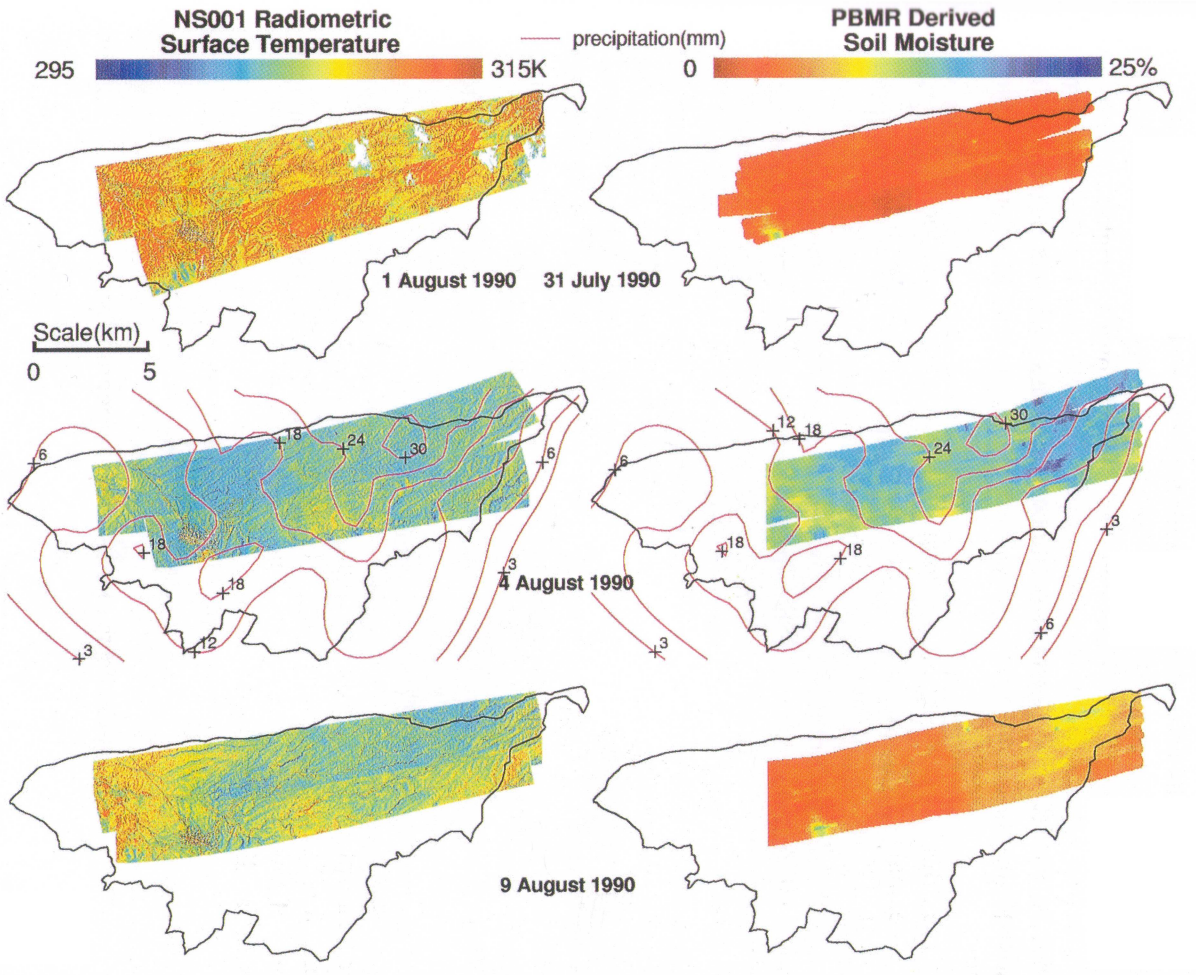

Figure 6.8. Push Broom Microwave Radiometer derived soil moisture, NS001 derived surface temerature (Humes et al., 1997), and accumulated precipitation for the WGEW during the Monsoon '90 experiment (Houser et al., 1998). The precipitation contours shown for August 4, 1990 show the precipitation that fell from multiple storms between August 1 and August 4.

of the ESTAR instrument for soil moisture estimation was established by this study (Jackson et al., 1993).

Soil moisture patterns in the WGEW, as observed by both in-situ and remote sensing, are complex, with large variability at all scales. However, some spatial structure is evident, arising from highly-localised convective precipitation, drydown processes, and surface characteristics such as soil and vegetation type.

6.2.3 Observed Spatial and Temporal Characteristics of Walnut Gulch Runoff

The interactions of rainfall patterns and antecedent soil moisture patterns will of course play a role in determining patterns of runoff generation. The nested structure of the runoff observation network within the WGEW affords an opportunity to examine spatial runoff patterns to some degree. In Figure 6.9 the runoff per unit area for each of the gauged catchments resulting from the August 1, 1990 storm is illustrated as a circle at the outlet of each gauged catchment whose size is proportional to the runoff magnitude. As expected, runoff was generated in regions of high rainfall. Sufficient runoff was generated from this event so that the flow was able to traverse approximately 15 km of dry ephemeral channel and reach the overall catchment outlet. While many of the catchments produced no runoff from the August 1, 1990 event, a more regular pattern of runoff distribution is observed for a ten year average (1969–1979). The general trend apparent in this data is a reduction in mean annual runoff per unit area with increasing drainage area.

These trends are consistent with the ephemeral semi-arid nature of the catchment where runoff is not augmented by ground water inflows. Without a saturated channel system, the dry loose alluvium present in the vast majority of the larger channels is able to absorb a significant volume of surface runoff. Depending on the location of rainfall, these channel transmission losses can also significantly impact peak runoff rates (Renard et al., 1993). An example

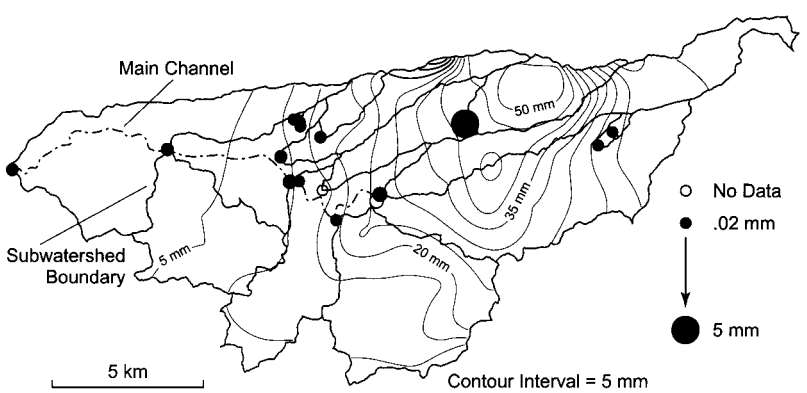

Figure 6.9. Runoff volumes and rainfall depths on Walnut Gulch from the storm of August 1, 1990.

of the impacts of channel transmission losses on runoff volume and peak runoff rate is illustrated in Figure 6.10 for the event of August 27, 1982. This figure depicts the storm isohyets and the hydrographs at flumes 6, 2, and 1. Because the rainfall is isolated above these flumes the change in hydrograph runoff volume and peak rate is solely attributed to transmission losses.

Channel transmission losses effectively decrease the correlation between rainfall and upland soil moisture patterns, and observed runoff. In the extreme case, all locally generated runoff may infiltrate into the channels. In this case any connection between rainfall and soil moisture patterns is severed downstream of the terminal location of the runoff front. Goodrich et al. (1997) concluded that explicit treatment of channel transmission losses is required for modelling catch-

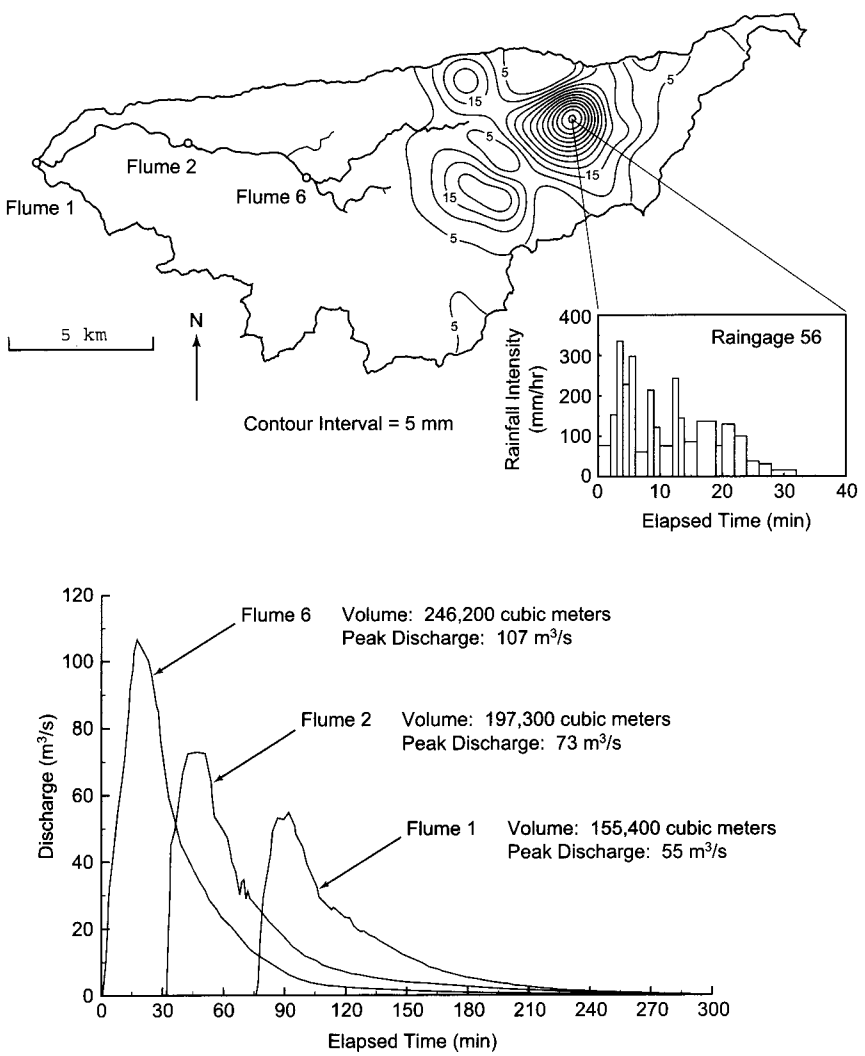

Figure 6.10. Storm total isohyets and hydrographs from flumes 6, 2, and 1 for event of August 27, 1982.

ments larger than roughly 40 hectares. In the case where two runoff events occur over the same reach of channel within a short period of time (< 3 days), runoff from the second event can be greatly enhanced as transmission losses are largely satisfied by the prior event.

6.3 MODELLING AND SPATIAL INFERENCES

6.3.1 Precipitation Modelling

Spatial precipitation modelling efforts posed and tested using WGEW data were initiated with extensions from point observations to area (Osborn, 1977); depth–area (Osborn and Lane, 1972); and, point–area frequency conversions (Osborn and Lane, 1981). These studies provide methods for areal distribution of rainfall uniformly without internal storm pattern information. Several stochastic models have also been developed to predict the spatial and temporal distribution of thunderstorm rainfall (Osborn et al., 1980; Eagleson et al., 1987; Islam et al., 1988; Jacobs et al., 1988). In general these models were able to reproduce the main statistical features of rainfall patterns. However, model stationarity assumptions limited model results as they were not able to describe observed nonstationary storm behaviour.

While these models have some utility in predicting rainfall patterns that are statistically similar to observations, the remotely sensed spatial patterns (Section 6.2.2) have the potential to estimate observed spatial rainfall patterns on an event basis. As noted in that section, Schmugge et al. (1994) found a high correlation of change in brightness temperature between flight acquisition dates and total inter-flight rainfall. The data from one set of PBMR flights in 1990 and two sets of ESTAR flights in 1991 are illustrated in Figure 6.11. As illu-

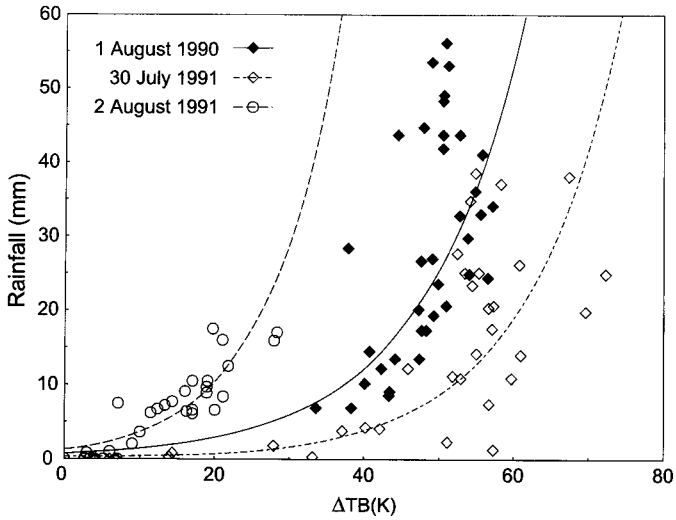

Figure 6.11. Relationship between raingauge total and decrease in brightness temperature (ΔTB) for three Walnut Gulch rainfall events. The lines are fitted exponential curves for the three events.

strated in the figure, a simple exponential model describes the relationship quite well. The respective R^2 values for this function are $R^2 = 0.68$, 0.83, and 0.79 for July 31 to August 2, 1990 (labelled August 1, 1990), July 30 to August 1, 1991 (labelled 30 July 1991) and August 2 to August 3, 1991 (labelled 2 August 1991) data. The variability in these relationships may be caused by differences in within-storm rainfall intensity patterns, infiltration, or evapotranspiration. The failure of the relationship above rainfall amounts of 30 mm is likely the result of two factors. First, for high rainfall amounts generating runoff, a portion of the rainfall is conveyed offsite and is concentrated in channels. In this case the full rainfall amount does not infiltrate and increase local soil moisture. The second factor has to do with the dynamic brightness temperature range of the L-band radiometer. For sparse vegetation the sensitivity of brightness temperature (TB) is about 2.5 K per percent of soil moisture. The dynamic range, given constant physical temperature, can be estimated by multiplying the sensitivity by the soil moisture range. Observed ranges of soil moisture vary from 18 % to almost 30 % depending on soil type. The corresponding dynamic range would vary from roughly 45 to 75 K.

The relationships illustrated in Figure 6.11 can be inverted to predict rainfall patterns. This analysis was carried out by Jackson et al. (1993) and comparison between observed rainfall patterns from the raingauge network and those predicted using the patterns of change in brightness temperature are illustrated for the two events in 1991 in Figure 6.12. The patterns predicted using changes in brightness temperature are very similar to patterns obtained from interpolating rainfall amounts from the dense raingauge network. As Jackson et al. (1993) note, for sparsely vegetated arid and semi-arid regions similar to Walnut Gulch, these results suggest the potential of using the change in brightness temperature method to estimate rainfall over large regions which do not have raingauge networks, provided a precipitation–ΔTB relationship is available.

6.3.2 Soil Moisture Modelling

6.3.2.1 Description of TOPLATS and its Application to Walnut Gulch

The TOPMODEL-based Land Atmosphere Transfer Scheme (TOPLATS) (Famiglietti and Wood, 1994) predicts spatial distributions of land surface runoff, energy fluxes, and soil moisture dynamics given atmospheric, soil, and vegetation information. It incorporates simple representations of atmospheric forcing, vertical soil moisture transport, plant-controlled transpiration, interception, evaporation, infiltration, surface runoff, and sensible and ground heat fluxes. The model incorporates a diurnal cycle and is driven with standard meteorological data with an hourly time step, this being considered sufficient to resolve the dynamics of the land–atmosphere interaction. The subsurface unsaturated soil column is partitioned into three layers, with the upper layer corresponding to the microwave remote sensing penetration depth, the underlying root zone extending from the bottom of the surface zone to the depth of

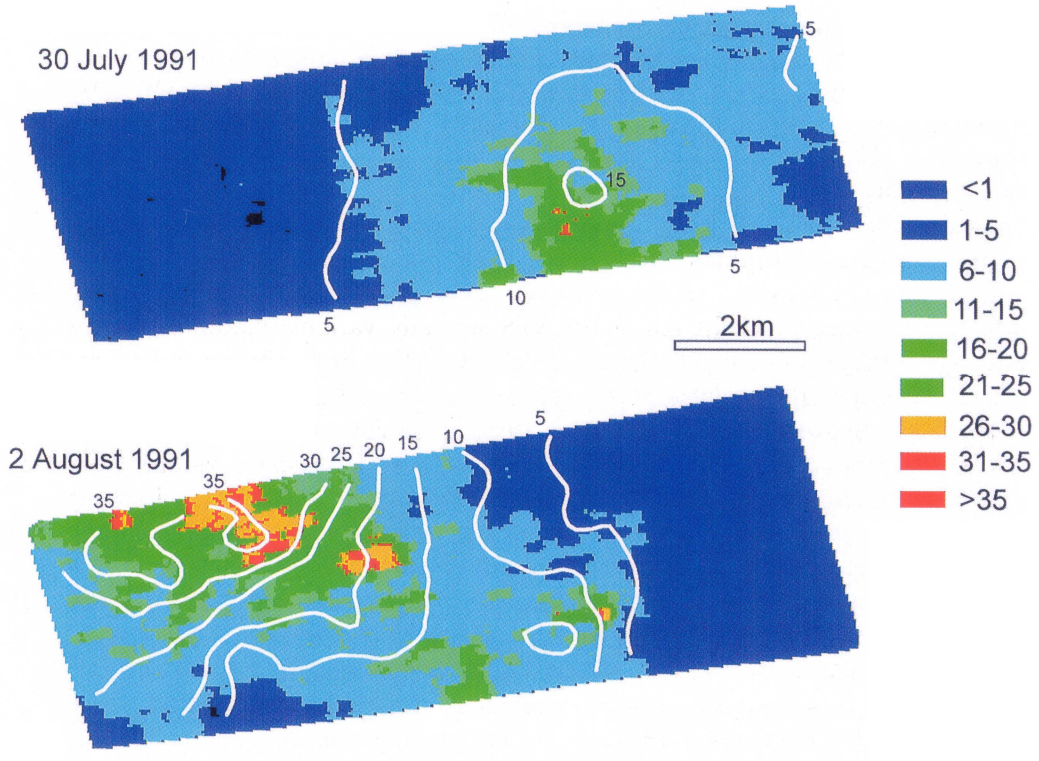

Figure 6.12. Rainfall maps for the Walnut Gulch study area. The isohyetal contour lines were derived from the observations made by the WGEW raingauge network. The images of predicted rainfall were obtained from the pre-storm to post-storm change in brightness temperature and the exponential models illustrated in Figure 6.11. All values are in mm. Top: July 30, 1991 event; Bottom: August 2, 1991 event. (Modified from Jackson et al., 1993.)

plant roots, and the transmission zone extending from the bottom of the root zone to the top of the saturated soil.

The WGEW was modelled using TOPLATS in a spatially distributed manner *at a 40 m resolution from July 23, 1990 to August 16, 1990. The TOPLATS* parameterisation was largely based on observations made during Monsoon '90 (Kustas and Goodrich, 1994). However, eight model parameters were not observed and had to be estimated or specified by model calibration (Houser et al., 2000).

6.3.2.2 Spatially Distributed Model Forcing and Parameters

The multiquadric precipitation interpolation algorithm (Syed, 1994) was used to produce spatially distributed precipitation values for the entire model domain from the available raingauge data. All other meteorological forcing (air temperature, wind speed, humidity, and radiation) were assumed to be spatially constant because observations from the eight Metflux stations contain insufficient infor-

mation to derive spatially-variable meteorological forcing for the approximately ninety thousand TOPLATS model grid points, and an eight-site average decreases the impact of highly local meteorologic signals (i.e., solar radiation measurement errors due to vegetation and topographic shading) on larger-area simulation. Therefore, meteorological forcing was derived from averaging observations at the eight Metflux stations in place during the experiment (Kustas and Goodrich, 1994).

It is thought that optimal implementation of a distributed hydrological model requires the specification of spatial distributions of soil and vegetation parameters. Therefore, the required TOPLATS spatially variable parameters were estimated using GIS maps of Walnut Gulch vegetation and soils; several examples of these spatially variable parameters are shown in Figure 6.13 and Houser et al. (2000). Spatially distributed information on minimum stomatal resistance, root depth, leaf area index, residual soil moisture, saturated soil moisture, saturated hydraulic conductivity, percent clay, percent sand, effective porosity, and topographic index at Walnut Gulch were used as parameters in the TOPLATS to make spatially distributed predictions. All other parameters were held spatially constant. The three TOPLATS soil moisture layers were initialised on July 23, 1990 based on catchment average in-situ TDR soil moisture observations.

The simulated spatial patterns of surface soil moisture at 12:00pm on August 7, 1990, using these spatially variable parameters, are shown in Figure 6.13. For comparison, the results for a simulation using spatially constant soil and vegetation parameters are also shown. The spatially variable soil and vegetation parameters have a large impact on the spatial patterns of the simulation, which appear unrealistic because they compare poorly with observed PBMR surface soil moisture. A series of sensitivity simulations was performed to determine which subset of spatial parameters contribute most to these patterns. The use of spatially variable vegetation parameters has much less effect on predictions as compared to soil parameters; it is likely that at the WGEW soil has more control of soil moisture processes than vegetation. The parameter specifying saturated soil moisture has the most influence on simulated spatial patterns, while those which specify the percentages of sand and clay, the saturated hydraulic conductivity, and the residual soil moisture have a more moderate influence. Finally, the spatially variable topographic index has very little influence on the simulations because the process of water table interaction with the surface does not operate at the WGEW.

The artefact of enhanced spatial soil and vegetation polygons apparent in the simulations is probably not a simple mis-specification of parameter values, rather it is an artefact of discretely assigning a single set of parameters (which in reality would display high variability, see for example Chapter 10, Figure 10.4) to large areas. A more appropriate specification of spatial parameters would be continuous, as obtained with remote sensing. It might be possible to develop a smoothing algorithm that would use the soil polygon information to approximate continuously varying, spatially distributed parameters. Because the simulations using spatially constant vegetation and soil parameters compare

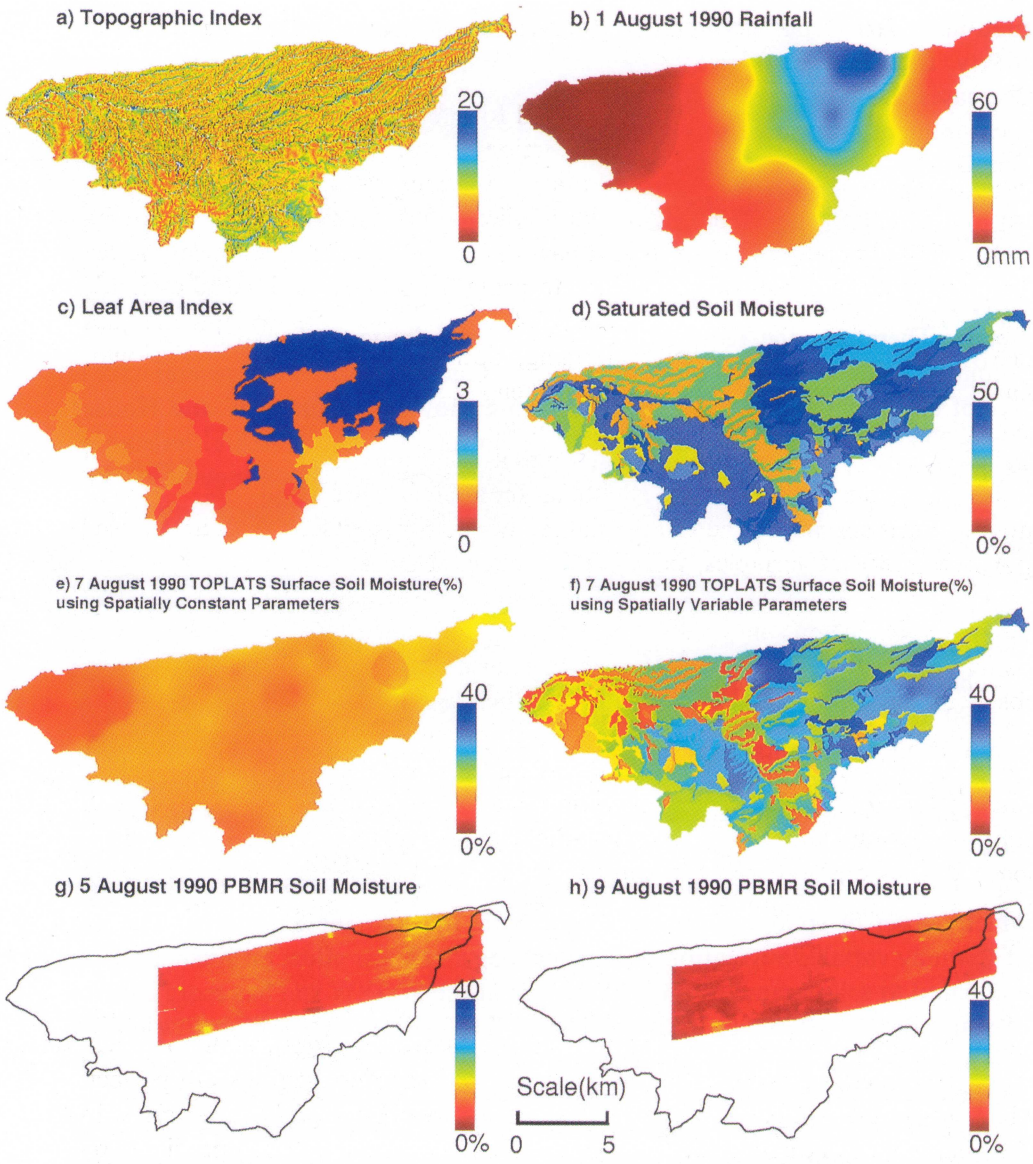

Figure 6.13. Spatially distributed topographic index (a); precipitation (b); vegetation (c); and soils (d); for the Walnut Gulch Experimental Watershed. TOPLATS spatial predictions of surface soil moisture at 12:00pm on August 7 1990 using spatially constant (e) and spatially variable (f) soils and vegetation parameters (all simulations use spatially variable topography and precipitation). Push Broom Microwave Radiometer (PBMR) derived soil moisture for August 5, 1990 and August 9, 1990 (Houser, 1996). The addition of spatially variable soils and vegetation produces unrealistic polygon artefacts in the simulation.

well to the PBMR patterns, soil and vegetation parameters were assumed spatially constant across the catchment in subsequent studies, leaving precipitation as the dominant spatially varying entity (topographic index is also variable, but with little effect).

6.3.2.3 Four-Dimensional Data Assimilation for Enhanced Soil Moisture Pattern Identification

Errors in the structure, parameters, and forcing of TOPLATS can never be fully rectified, and therefore lead to prediction errors. However, observations of model states or storages, distributed in time and space, can be used to correct the trajectory of the model, and reduce its prediction errors. Charney et al. (1969) first suggested combining current and past data in an explicit dynamical model, using the model's prognostic equations to provide time continuity and dynamic coupling amongst the fields. This concept has evolved into a family of techniques (i.e., direct insertion, Newtonian nudging, optimal interpolation, variational, Kalman filtering, etc.) known as Four-Dimensional Data Assimilation (4DDA). TOPLATS was modified to allow the assimilation of soil moisture and other state variables. The following description assumes assimilation of observed surface soil moisture, θ_o, derived from the PBMR (as shown in Figure 6.8). However, with modifications specific to the state variable, the following description can be used to assimilate other variables, such as surface temperature.

A control and a direct insertion simulation are used as the basis for evaluating the data assimilation runs. A control simulation (i.e., the simulation without data assimilation) can be considered an extreme case, in which it is assumed that the observations contain no information. The other extreme is direct insertion, where it is assumed that the model contains no information. In this case, the model prediction of surface soil moisture, θ_{sz}, is replaced with a PBMR soil moisture observation, θ_o, whenever an observation is available. With direct insertion, no data are assimilated outside the four-dimensional region (one time and three space dimensions) where observations are available; therefore, any advection of information is only accomplished via the model physics in subsequent model integrations.

In a second data assimilation technique, which is termed "statistical correction", the mean and standard deviation of the surface soil moisture states in the model are adjusted to match the mean and standard deviation of the observations. This method assumes that the statistics of the observations are perfect, which is arguably more reasonable than assuming that each observation is in itself perfect, as in direct insertion. It also assumes that the patterns predicted by the model are correct but that the predicted surface soil moisture statistics contain bias. As with direct insertion, advection of information into deeper soil layers is accomplished solely through the model physics.

A third data assimilation technique called Newtonian nudging relaxes the model state towards the observed state by adding an artificial tendency term into the prognostic equations which is proportional to the difference between the two states. These small forcing terms gradually correct the model fields which are assumed to remain in approximate equilibrium at each time step (Stauffer and Seaman, 1990). In this way, the model can be nudged toward observations within a certain distance, and during a period of time, around the observations. Newtonian nudging is implemented as follows:

$$\frac{\partial \theta}{\partial t} = F(\theta, x, t) + G_\theta \cdot W_\theta(x, t) \cdot \varepsilon_\theta(x) \cdot (\theta'_o - \theta) \tag{6.1}$$

The model's forcing terms are represented by F, θ'_o is the PBMR surface soil moisture observation at the model grid, and t is time. G_θ is the nudging factor which determines the magnitude of the nudging term relative to all other model processes, while the four-dimensional weighting function, W_θ, specifies its spatial and temporal variation. The analysis quality factor, ε_θ, varies between 0 and 1 and is based on the quality and distribution of the observations. Equation (6.1) was implemented for all three TOPLATS soil layers.

The Newtonian nudging weighting function, W, at time, t, and location, x, for each observation, I, is a combination of the horizontal weighting function, w_{xy}, the vertical weighting function, w_z, and the temporal weighting function, w_t, thus:

$$W(x, t) \equiv w_{xy} \cdot w_z \cdot w_t \tag{6.2}$$

The horizontal weighting function can be defined by a Cressman-type horizontal weighting function, as:

$$w_{xy} = \frac{R^2 - D^2}{R^2 + D^2}, \qquad 0 \leq D \leq R \tag{6.3}$$

$$w_{xy} = 0, \qquad D > R \tag{6.4}$$

where R is the radius of influence, and D is the distance from the i^{th} observation to the gridpoint. The vertical weighting function, w_z, is also a distance weighting function, following Seaman (1990); thus:

$$w_z = 1 - \frac{|z_{obs} - z|}{R_z}, \qquad |z_{obs} - z| \leq R_z \tag{6.5}$$

$$w_z = 0, \qquad |z_{obs} - z| > R_z \tag{6.6}$$

where R_z is the vertical radius of influence, and z_{obs} is the vertical position of the i^{th} observation. The temporal weighting function is defined as follows:

$$w_t = 1, \qquad |t - t_0| < \frac{\tau}{4} \tag{6.7}$$

$$w_t = 0, \qquad |t - t_0| > \tau \tag{6.8}$$

$$w_t = \frac{(\tau - |t - t_0|)}{\tau/4}, \qquad \frac{\tau}{4} \leq |t - t_0| \leq \tau \tag{6.9}$$

where t is the model-relative time, t_0 is the model-relative time of the i^{th} observation, and τ is the half-period of a predetermined observation influencing time window.

The final data assimilation method explored here is statistical or optimal interpolation, which is a minimum variance method that is closely related to kriging. Statistical interpolation was implemented in all three TOPLATS soil layers as follows (Daley, 1991):

$$\theta_A(r_i) = \theta_B(r_i) + \sum_{k=1}^{K} W_{ik} \cdot [\theta_O(r_k) - \theta_B(r_k)] \tag{6.10}$$

where K is the number of observation points, W_{ik} is the weight function, $\theta(r)$ is the soil moisture analysis variable, r is the three-dimensional spatial coordinates, $\theta_A(r_i)$ is the analysed value of θ at the analysis gridpoint r_i, $\theta_B(r_i)$ is the background or first-guess value of θ at r_i, and $\theta_O(r_k)$ and $\theta_B(r_k)$ are the observed and background values, respectively, at the observation station r_k.

The weight function, W_{ik}, is determined by least-squares minimisation of equation (6.10), with the assumptions that $\theta_B(r_k)$, $\theta_B(r_i)$, and $\theta_O(r_k)$ are unbiased, that there is no correlation between the model and observation error, that the error correlations are homogeneous, isotropic, and time invariant, and that the background error correlation, ρ_B, is horizontally and vertically separable (i.e., $\rho_B = \rho_{Bxy}\rho_{Bz}$) (Daley, 1991), thus:

$$\sum_{l=1}^{K} W_{il} \cdot \left[\rho_{Bxy} \cdot (r_l - r_k) + \varepsilon_O^2 \cdot \rho_O \cdot (r_l - r_k)\right] = \rho_{Bxy} \cdot (r_i - r_k) \cdot \rho_{Bz} \cdot (z_i - z_k) \tag{6.11}$$

where ρ_O is the observation error correlation matrix, ρ_{Bxy} is the background horizontal error correlation matrix, and ρ_{Bz} is the vertical error correlation matrix. ρ_O and ρ_B were estimated using PBMR observations and corresponding model predictions (Houser et al., 1998). The system of linear equations given in equation (6.11) was solved using a Cholesky Decomposition (Press et al., 1986). Each PBMR image contains over 35,000 observations, which requires solving a system of 35,000 linear equations for each model grid point each time an observation was available. Clearly the computational resources needed for this task are unreasonable; hence, a simplified method was required. This was accomplished by (a) using a random subset of 100 PBMR observations, and (b) by using 100 "super-observations", these being approximately 1 km^2 PBMR soil moisture averages.

Catchment average time series of surface and root zone soil moisture for the various assimilations using all of the available PBMR observations are shown in Figure 6.14. All of the data assimilation methods significantly and similarly improved the simulation of surface zone soil moisture, with the exception of direct insertion, which was unable to impose an entire catchment correction and was therefore unable to adjust the model trajectory sufficiently. Nudging had the clear advantage of providing smoother temporal adjustments. All simulations produced identical surface zone soil moisture simulations after the storm on August 12, 1990 because this storm saturated the surface zone causing all past surface zone forcing to be forgotten, but this process does not occur in the model's root zone where memory of past assimilation is preserved. This sequence of events is not unrealistic; rather, it suggests a time interval at which soil moisture observations are needed for data assimilation, this interval being less than or equal to the time between storm events. In the root zone, the simulated time

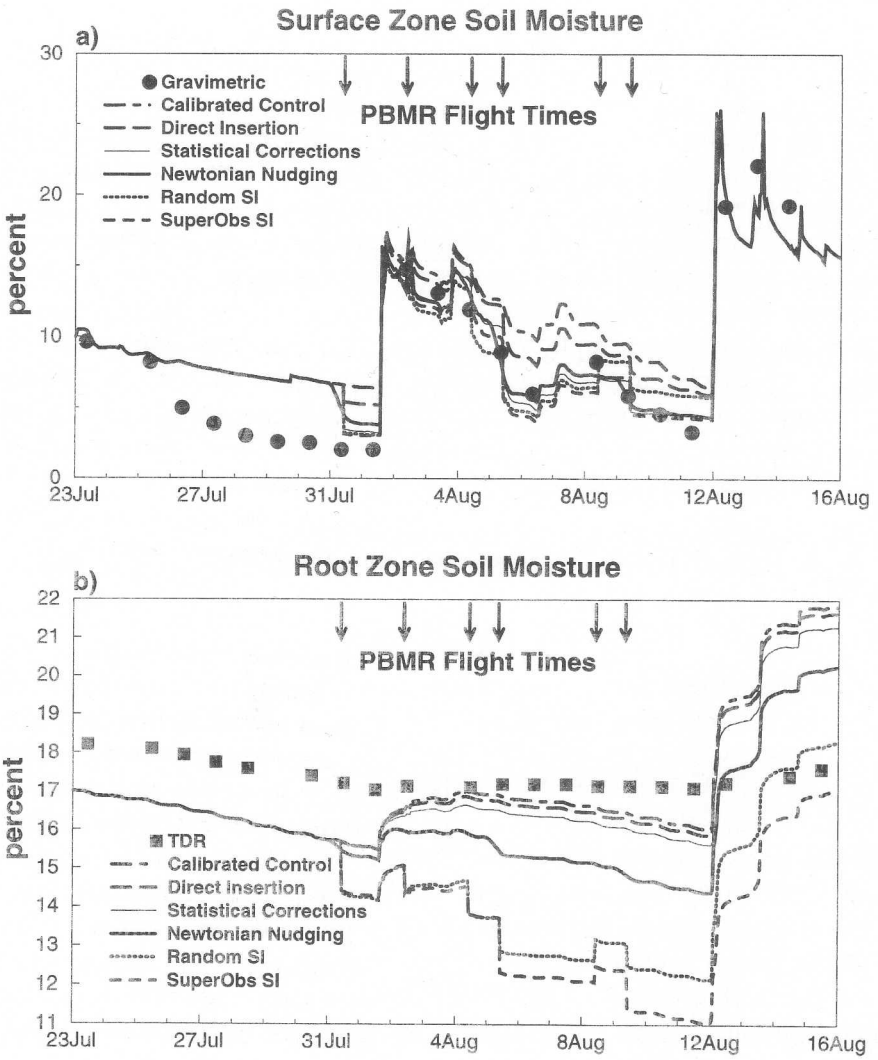

Figure 6.14. Comparison of TOPLATS catchment average surface and root zone soil moisture time series for various assimilation studies. (From Houser et al., 1998; reproduced with permission.)

series fell into two distinct groups corresponding to methods with and without the capability for vertical assimilation of information. Among the latter group, nudging assimilation performs a more conservative correction compared to statistical interpolation. None of the methods produced time series that matched the in-situ root zone observations. However, it is important to bear in mind that with only two in-situ root zone observations, the root zone spatial variability is not adequately sampled.

The control run deviates most significantly from observations near the end of the drydown on August 7, 1990, so this time is selected to demonstrate the intercomparison between assimilation methods. It should be noted that four

PBMR images were assimilated prior to this time, with the last assimilation occurring on August 5, 1990. The spatial patterns of model-predicted surface soil moisture for the different assimilation methods are shown in Figure 6.15. The best spatial patterns are considered to be those without discontinuity at the edge of the observed area, without numerical artefacts, and with a similar nature to those produced by the model without assimilation.

Simple updating is unable to advect information horizontally, giving rise to an undesirable discontinuity in the calculated soil moisture field and preserving all the observational noise. Updating also is able only to impact root zone soil moisture very slightly through model physics and preserves the discontinuity in this zone. Data assimilation via statistical corrections is able to adjust the entire surface soil moisture field to observed levels. It produces a soil moisture spatial field that does not contain discontinuities or retain the observed spatial pattern. Newtonian nudging also produces a spatial field of soil moisture without discontinuities.

Both the random and the super-observation statistical interpolation approaches result in an undesirable linear streaking feature that extends outward from the observed area that is an artefact of numerical procedures, or may be the result of a violation of the statistical interpolation unbiased background assumption. Statistical interpolation has the advantage of using error correlation functions based on the characteristics of the observations and the model predictions. However, it also has the disadvantage of being excessively demanding on computer resources when addressed as a fully posed problem with remotely sensed data, and it lacks the benefits of temporal assimilation.

There is a clear tradeoff between using a complex data assimilation technique and the ability to use all the available data due to the large computational burdens of performing data assimilation at fine resolutions using dense data sets. As the complexity of the data assimilation model increases, the size of the assimilated data set needs to decrease in order to maintain computational feasibility. Complex methods have the ability to extract more useful information from assimilated data, but simpler methods use more of the data to extract similar information. This tradeoff allows simpler assimilation techniques to perform almost as well as complex techniques. In general, this argument suggests the use of assimilation methods that are of moderate complexity, that are sound and computationally efficient, but use as much data as possible. If the information in the data can be efficiently compressed or filtered before its use in data assimilation, and if the mathematical solvers can be further optimised, it may be reasonable to use larger data sets in complex data assimilation strategies.

6.3.3 Runoff Modelling

The range of runoff models applied to, or developed with, Walnut Gulch data varies widely in both complexity and type. Early models included those based on linear regression at annual time scales (Diskin, 1970) and stochastic models for estimating the start of the runoff season, the number of runoff events per season,

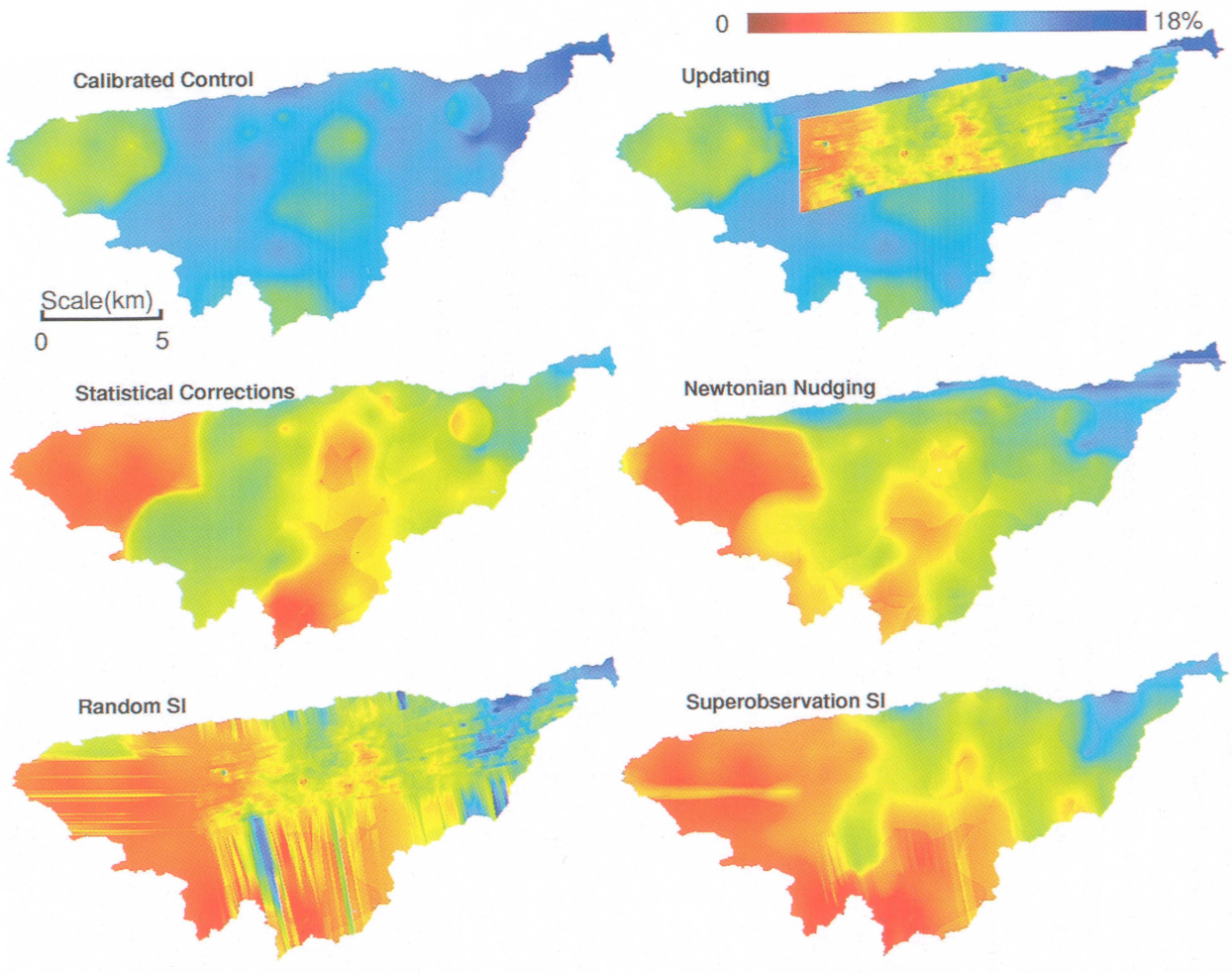

Figure 6.15. Comparison of TOPLATS spatial surface zone soil moisture at 12:00pm on August 7, 1990 from various assimilation methods. (From Houser et al., 1998; reproduced with permission.)

time interval between events, beginning event time, runoff volume, and peak discharge (Diskin and Lane, 1972; Lane and Renard, 1972). More geometrically detailed recent work by Syed (1994) further reinforced the importance of spatial distributions of both rainfall and pre-storm soil moisture availability on catchment runoff response using the 302 storm events discussed earlier with regression analyses. Simple measures of spatial characteristics of rainfall considered individually did not show a very high degree of correlation with either runoff volume or peak rate of runoff for WG1 (the whole experimental catchment). The highest correlation, R^2, was found to be between precipitation volume and runoff volume ($R^2 = 0.59$) and precipitation volume and peak rate of runoff ($R^2 = 0.53$). However, when only the precipitation volume of the storm core (intensities > 25 mm/hr) was considered, the coefficients of correlation increased to 0.71 and 0.76, respectively. This clearly illustrates that the high-intensity portions of the storm core are directly related to runoff production.

A large number of other models have also utilised data from Walnut Gulch for development or validation. These include CREAMS (Knisel, 1980); SPUR (Lane, 1983a,b; Renard et al., 1993); ARDBSN (Stone et al., 1986); WEPP (Lopes et al., 1989); and CELMOD5 (Karnieli et al., 1994). A particularly well adapted model for use in arid and semi-arid regions where transmission losses are important was developed by Lane (1982).

6.3.3.1 Description of KINEROS and Its Application to Walnut Gulch

KINEROS is a physically based, event-oriented kinematic runoff and erosion model (Smith et al., 1995) that was also developed and tested using WGEW data. In this model, catchments are represented by discretising contributing areas into a cascade of one-dimensional overland flow and channel elements using topographic information. The infiltration component is based on the simplification of the Richard's equation posed by Smith and Parlange (1978):

$$f_c = K_s \frac{e^{F/B}}{(e^{F/B} - 1)}; \qquad \text{and} \qquad B = G \cdot \varepsilon \cdot (S_{\max} - SI) \tag{6.12}$$

where f_c is the infiltration capacity (L/T), K_s is the saturated hydraulic conductivity (L/T), F is the infiltrated water (L), B is the saturation deficit (L), G is the effective net capillary drive (L), ε is the porosity, $S_{\max}$ is the maximum relative fillable porosity, and SI is the initial relative soil saturation. Runoff generated by infiltration excess is routed interactively using the kinematic wave equations for overland flow and channel flow, respectively stated as:

$$\frac{\partial h}{\partial t} + \frac{\partial \alpha \cdot h^m}{\partial x} = r_i(t) - f_i(x, t); \quad \text{and} \quad \frac{\partial A}{\partial t} + \frac{\partial Q(A)}{\partial x} = q_l(t) - f_{c_i}(x, t) \tag{6.13}$$

where h is the mean overland flow depth (L), t is time, x is the distance along the slope (L), α is 1.49 $S^{1/2}/n$, S is the slope, n is Manning's roughness coefficient, m is 5/3, $r_i(t)$ is the rainfall rate (L/T), $f_i(x, t)$ is the infiltration rate (L/T), A is the channel cross-sectional area of flow (L^2), $Q(A)$ is the channel discharge as a

function of area (L^3/T), $q_l(t)$ is the net lateral inflow per unit length of channel (L^2/T), and $f_{ci}(x, t)$ is the net channel infiltration per unit length of channel (L^2/T). These equations, and those for erosion and sediment transport, are solved using a four-point implicit finite difference method (Smith et al., 1995).

Unlike excess routing, interactive routing implies that infiltration and runoff are computed at each finite difference node using rainfall, upstream inflow, and current degree of soil saturation. This feature is particularly important for accurate treatment of transmission losses with flow down dry channels. To explicitly account for space-time variations in rainfall patterns the model computes, for each overland flow element, the rainfall intensities at the element centroid as a linear combination of intensities at the three nearest gauges forming a piece-wise planar approximation of the rainfall field over the catchment (Goodrich, 1990). The interpolated centroid intensity is applied uniformly over that individual model element. To represent small-scale variability of infiltration that is beyond the scale of discretisation (sub-metre to metre), the model assumes the saturated hydraulic conductivity (K_s) within an overland flow element varies log-normally (Woolhiser and Goodrich, 1988; Smith et al., 1990) (i.e., it uses a sub-grid distribution function parameterisation as discussed in Chapter 3).

Validation of the KINEROS model is reported by Goodrich (1990), Goodrich et al. (1993), and Smith et al., (1995) on four Walnut Gulch subcatchments (Lucky Hills (LH)-106, 0.4 ha; LH-102, 1.4 ha; LH-104, 4.4 ha; and WG-11, 631 ha). For the Lucky Hills catchment, rainfall inputs were obtained from two raingauges, and for WG-11 ten raingauges were used. The validation process consisted of a split sample test (Chapter 3, p. 76 and Chapter 13, p. 340) with the calibration phase using approximately ten observed events on each catchment and a validation phase in which an independent set of roughly twenty runoff events were used to assess model performance using the coefficient of efficiency, E (Nash and Sutcliffe, 1970) (Table 6.1). The model was calibrated by adjusting

Table 6.1. KINEROS calibration and verification coefficient of efficiency for runoff volume and peak discharge

Basin	Calibration efficiency						Verification efficiency				Maximum no. of model elements
	Volume			Peak			Volume		Peak		
	1	2	3	1	2	3	1	2	1	2	
LH-6	0.98	0.97	0.81	0.95	0.94	0.86	0.98	0.98	0.79	0.77	30
LH-2	0.97	0.88	0.88	0.97	0.93	0.93	0.93	0.92	0.93	0.89	68
LH-4	0.97	0.96	0.89	0.98	0.88	0.88	0.99	0.99	0.92	0.96	235
WG-11	0.86			0.84			0.49		0.16		243

1 – two raingauges in Lucky Hills, ten raingauges in WG-11, using the maximum number of overland and channel flow elements
2 – two raingauges, one overland flow element, no channel elements
3 – one raingauge, maximum number of overland and channel flow elements
* – If the model predicts observed runoff with perfection, $E = 1$. If $E < 0$, the model's predictive power is worse than simply using the average of observed values.

three parameters: basin-wide multipliers on n, K_s, and CV_{Ks}. The multipliers scale the model element input parameters while maintaining relative differences based on field observations. Using this approach, the overall dimension of the adjustable parameter space remains small (see Chapter 13, pp. 342–3 for a discussion of this approach). By using the nested catchments LH-106 and LH-102 (see Figure 6.1) within catchment LH-104, internal assessment for the model's ability to reproduce runoff patterns was also possible.

As judged by the efficiency statistics, the model provides remarkably good predictions of runoff volume and peak response for the Lucky Hills catchments. An overall assessment of internal model accuracy using the nested catchments gives an E of 0.91 and 0.86 for LH-106 runoff volume and peak rate, respectively, and comparable LH-102 E values of 0.96 and 0.97. These high values of E obtained by using LH-104 multipliers for the internal catchments suggest a good deal of internal model accuracy. On WG11 the model performed reasonably well for the calibration event set, but E dropped off considerably for the verification event set due to overprediction of the two largest events in the verification set.

While we can represent a wide range of geometric catchment complexity, it is not clear just how much is required to best represent hydrological response. Does the use of a great number of model elements, and therefore a great amount of distributed input, actually improve the simulations or can simpler geometries do just as well? Which components can be simplified and which must have their spatial detail preserved? Geometric model complexity and catchment heterogeneity are closely related. More complex model representations (i.e., more overland flow and channel model elements) more closely preserve the catchment patterns of topography and channel networks. Large-scale orthophoto maps were used to discretise the catchments into a large number of elements, and a geometric simplification procedure based on stream order reduction was developed (Goodrich, 1990). Successive levels of reduction in model complexity were then carried out to assess the impacts of simplification on simulated runoff response. It was found that adequate representation of concentrated channel routing imposed a fundamental limit on simplification because concentrated channel flow can only be converted to overland flow with a distortion of the hydraulic roughness to a certain degree. For catchments greater than 1 hectare it was found that an average area for first-order channels should be roughly 10–15% of the total catchment area (Goodrich, 1990).

The relative impact of geometric versus rainfall pattern simplification was also assessed. The error introduced when the model was simplified to a single overland flow plane with two raingauges as input was less than or equal to the error when one raingauge was used in the Lucky Hills catchments as input to a model with the maximum number of elements corresponding to the most complex geometric catchment representation (see Table 6.1). This result was even more pronounced in the larger WG-11 catchment when one versus ten raingauges was used (Goodrich, 1990). *Therefore, unless there are major differences in land use, basin discretisation should not exceed the ability to resolve input rainfall variability.*

The uncertainty in rainfall input due to small- and large-scale spatial variability suggests that the confidence in the calibration can only be equal to or less than the certainty of rainfall input data.

Faurès et al. (1995) assessed the impacts of Walnut Gulch rainfall variability on runoff simulations in the LH-104 catchment using KINEROS (Figure 6.16). Data from combinations of five recording raingauges were input into KINEROS for the event of August 3, 1990. These simulations produced a range of variation for simulated peak runoff rate and runoff volume of 15 mm/hr ($CV = 38.8\,\%$) and 2.6 mm ($CV = 40.0\,\%$), respectively. The variability in runoff model results emphasises the importance of adequately sampling the spatial distribution of rainfall in the catchment. It was also found that model output variation as a function of the number of raingauges was generally greater for small events than for large ones. This reflects the difficulty of modelling small runoff events when runoff to rainfall ratios are low and measurement error may be a larger relative percentage of the input rainfall signal. This would be expected whenever relative infiltration and rainfall rates are close, resulting in small runoff ratios. In this case, the model becomes very sensitive to both input and parameter patterns. If the uniform, single raingauge assumption were used during parameter fitting in spite of spatial variability comparable to that observed here, the variation in simulated hydrographs

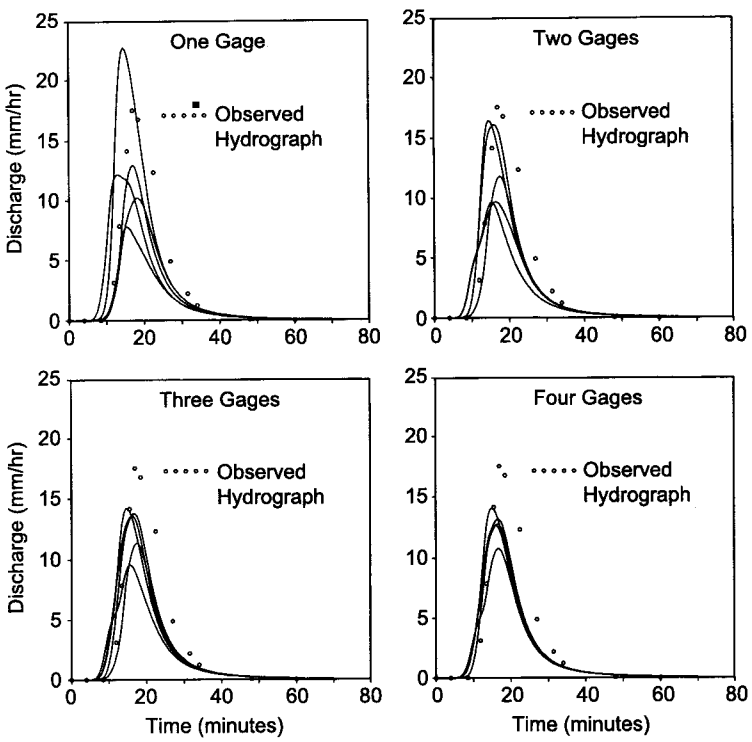

Figure 6.16. Simulated hydrographs for five combinations of one, two, three, and four raingauges in Lucky Hills-104 (August 3, 1990 event).

could be mistakenly assigned to variability of other model parameters or errors in the model structure.

Finally, the relative importance of PBMR derived remotely sensed soil moisture patterns (Section 6.2.2) on runoff simulations on the larger WG-11 catchment is examined. KINEROS is very sensitive to the estimate of the pre-storm initial relative soil saturation, *SI* (Goodrich, 1990). An average *SI* was derived for each of 256 model elements (3.4 ha mean overland flow element area) from five PBMR overflights, three of which are illustrated as volumetric soil moisture in Figure 6.8 (Goodrich et al., 1994). An increase in the variability of *SI* with increasing mean *SI* was observed; however, the highest mean *SI* observed was 0.45 on a zero to one scale, so the generally postulated decrease in variability as *SI* approaches one was not observed (Goodrich et al., 1994). Attaining a very high average *SI* may not be realised given the rapid drainage of the coarse soils of WG-11 and the difficulty of obtaining an aircraft overflight immediately following an intense convective thunderstorm.

In order to assess the relative importance of variability in initial soil saturation and variability in precipitation, a simulation study was performed using different combinations of observed patterns in soil saturation (from PBMR data) and precipitation (from multiple raingauges). The impact of simplifying the representation of initial soil saturation was assessed by comparing the highly complex *SI* pattern (256 *SI* values) to a single catchment average *SI* representation (Figure 6.17). For rainfall simplification, the case of using observations from ten raingauges in and near the catchment is compared to using rainfall from a single central raingauge (uniform rainfall). The rationale for using *average SI* but a *single* raingauge (rather than average of the ten, which would be less variable) is

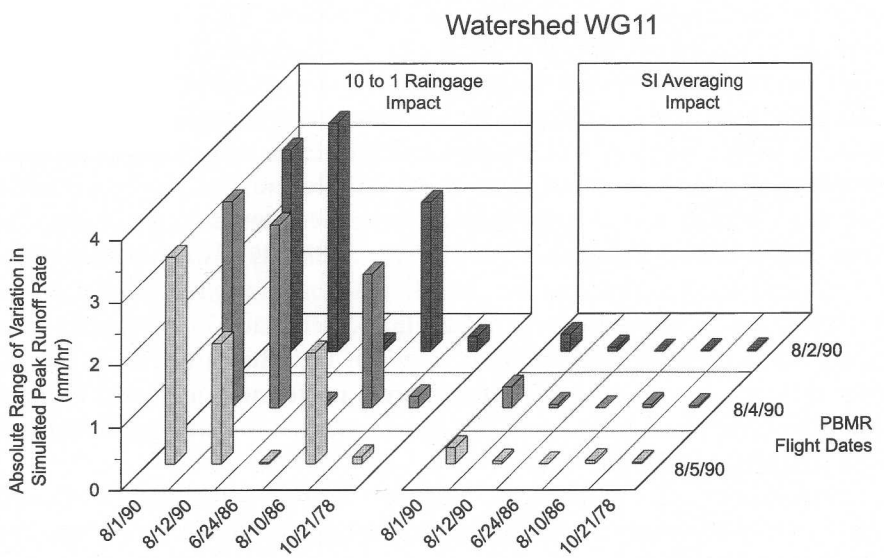

Figure 6.17. Impacts of PBMR initial soil moisture (SI) averaging and rainfall representation on simulated peak runoff rate for various storm–SI combinations.

that average *SI* data may become widely available from low spatial resolution sensors, while only single raingauges are usually available and applied uniformly to large areas.

The comparisons were made for three PBMR derived sets of *SI* (August 2, 4, and 5, 1990) and for five storms, two of which occurred during the period of PBMR overflights and three historical storms that had relatively small runoff volumes and distinct rainfall patterns. The October 21, 1978 event was relatively uniform, the June 24, 1986 event had high rainfall gradients in the upper central portion of WG11, and the August 10, 1986 event produced steep precipitation gradients in the lower portion of WG11. The magnitude of these storm/runoff events means that the influence of *SI* on runoff generation is large because the rainfall depth is of the same order as the soil water deficit (Goodrich, 1990). The absolute percentage change in peak runoff rate ranged from 0.5 % to 12.3 % for *SI* averaging and over 400 % for rainfall simplification. Based on these results, a simple basin average of remotely derived *SI* estimates at the medium catchment scale (6.31 km^2), with a greater knowledge of spatial rainfall patterns, appears to be adequate for runoff simulation. This implies that the relatively coarse resolution of potential space-based microwave instruments may be entirely adequate for defining distributed pre-storm initial soil water content conditions for rainfall-runoff modelling in semi-arid regions, provided ground truth data are available (Goodrich et al., 1994).

6.4 CONCLUSIONS

Our understanding of the complex hydrological processes active in semi-arid regions has been greatly enhanced through numerous studies of rainfall, runoff, and soil moisture patterns at the USDA-ARS Walnut Gulch Experimental Watershed in southeastern Arizona. Extremes in rainfall and temperature in this region lead to great spatial heterogeneity in soil hydrological processes. Accurate spatial and temporal knowledge of precipitation totals and intensity were found to be the most important factor in determining hydrologic catchment patterns in this region. Convective rainfall is highly localised with observations indicating that rainfall from raingauges six or more kilometres apart can be considered independent. Significant rainfall variability is also apparent over scales of several hundred metres as rainfall gradients ranging from 0.28 to 2.48 mm/100 m were observed over a 4.4 hectare catchment. This suggests that the typical uniform rainfall assumption is *invalid* at the 5 hectare scale in this or similar environments. Soil moisture patterns were profoundly impacted by precipitation. Remote sensing techniques also show potential for indirect estimation of rainfall at ungauged catchments.

The correlation structure present in the PBMR derived soil moisture changes as the surface dries following a rain storm. Storms impose large-scale correlation which decreases as the soil dries and the random (small-scale) effects of surface characteristics begin to control soil moisture variability.

The techniques of data assimilation were successfully applied to obtain better soil moisture estimates using a distributed model and remote sensing data. Overall, the Newtonian nudging method has the most desirable features for remotely sensed soil moisture data assimilation. It is the only true four-dimensional data assimilation method used in this study, and it produces relatively continuous soil moisture time series and reasonable spatial patterns. There is a clear tradeoff between using a complex data assimilation technique and the ability to use all the available data. The use of assimilation methods that are sound and computationally efficient and use as much data as possible is preferred.

The relationships between storm size, location and pattern, and the scale and geometry of the catchment are delicate and should be carefully considered when interpreting or modelling hydrological processes. A critical process in this region is ephemeral channel transmission losses. Spatially distributed models that explicitly treat runoff routing and channel abstractions are considered essential. This is supported by good calibration and verification results of models with explicit physically-based routing and infiltration components using the nested gauge data.

The conclusions described here must be considered in the context of the semiarid Walnut Gulch environment. It should be reiterated that runoff is almost exclusively generated via an infiltration excess mechanism and annual potential evapotranspiration is roughly ten times greater than annual rainfall in this environment. In this influent environment, with annual runoff decreasing with increasing catchment size, it was found that runoff response becomes more nonlinear with increasing catchment size. Our increased understanding of this environment would not have been possible without the long-term, spatially dense observations made at the WGEW. We strongly encourage the continued operation and improvement of this exceptional outdoor laboratory.

ACKNOWLEDGEMENTS

We gratefully acknowledge the staff of the USDA-Southwest Watershed Research Center for their diligent collection, processing and interpretation of high-quality data from the Walnut Gulch Experimental Watershed. We also thank T. Jackson for providing several figures, and C. Unkrich for the preparation of many of the figures. We would also like to gratefully acknowledge support for the third author from the NASA/EOS grant NAGW2425.